Development/Plasticity/Repair

Formation of Whisker-Related Principal Sensory Nucleus-Based Lemniscal Pathway Requires a Paired Homeodomain Transcription Factor, *Drg11*

Yu-Qiang Ding,[1,2,3] Jun Yin,[1,2,3] Hai-Ming Xu,[1,2,3] Mark F. Jacquin,[4] and Zhou-Feng Chen,[1,2,3]

Departments of [1]Anesthesiology, [2]Psychiatry, [3]Molecular Biology and Pharmacology, and [4]Neurology, School of Medicine, Washington University, St. Louis, Missouri 63110

Little is known about the molecular mechanisms underlying the formation of the principal sensory nucleus (PrV) of the trigeminal nerve, a major relay station for somatotopic pattern formation in the trigeminal system. Here, we show that mice lacking *Drg11*, a homeodomain transcription factor, exhibit defects within the PrV, which include an aberrant distribution of *Drg11*$^{-/-}$ cells, altered expression of a molecular marker, unusual projections of primary afferents from trigeminal ganglion cells, and, subsequently, increased cell death. In addition, surviving PrV cells exhibit delayed and more spatially restricted ascending projections to the ventral posterior medial nucleus of the thalamus (VPm). These early embryonic abnormalities in the PrV lead to the failure to develop whisker-related patterns in the PrV, VPm, and somatosensory cortex. By contrast, somatotopic patterns exist in the spinal trigeminal subnuclei interpolaris (SpVi) and subnuclei caudalis (SpVc) and the dorsal column nucleus-based lemniscal and cortical pathway. Thus, the deficits in the trigeminal system of *Drg11*$^{-/-}$ mice are specific to the PrV. Our results demonstrate that *Drg11* is essential for proper cellular differentiation and, subsequently, for the formation of the whisker-related lemniscal and cortical structures.

Key words: **transcription factor; *Drg11*; barrel; principal sensory nucleus; subnucleus interpolaris; subnucleus caudalis; subnucleus oralis; morphogenesis**

Introduction

The somatosensory map of the periphery is represented at different levels of the brainstem, thalamus, and somatosensory (S1) cortex. On the face of rodents, whiskers are organized in a reliable array. This pattern is relayed via the axons of trigeminal ganglion (TG) neurons to the cells in the trigeminal brainstem nuclei, which in turn project to the thalamus and to the S1 cortex via the thalamocortical afferents (TCAs) (Woolsey and Van der Loos, 1970; Woolsey, 1990). The sensory map of the rest of the body is relayed by afferents of dorsal root ganglion neurons to the dorsal column nucleus (DCN), which projects to the contralateral ventral posterior lateral (VPl) nucleus of the thalamus and to the S1 cortex via TCAs (Killackey et al., 1990; Willis and Coggeshall, 1991; Tracey and Waite, 1995). In the trigeminal system, the whisker-related patterns occur in the principal sensory nucleus (PrV), subnuclei interpolaris (SpVi), and subnuclei caudalis (SpVc). The PrV-based lemniscal pathway and the SpVi-based paralemniscal pathway represent two parallel pathways that relay whisker-related information from the periphery to the cortex (Bates and Killackey, 1985; Diamond et al., 1992).

The well described somatotopic pattern in the trigeminal brainstem complex and its convenient detection make it one of the most attractive systems for studying fundamental mechanisms that control neuronal connection and pattern formation. Insofar as the whisker-related patterns are clearest during early postnatal periods, much of our knowledge regarding the formation of whisker-related patterns has been obtained by surgical manipulation of the periphery in postnatal animals (Woolsey, 1990). These studies indicate that the periphery plays an instructive role in somatotopic pattern formation (Killackey et al., 1990; Woolsey, 1990). Moreover, because lesions of the PrV lead to an absence of whisker-related patterns at higher levels of the brain, and lesions of the SpVi do not, the PrV has an indispensable role in thalamic and cortical patterning (Killackey and Fleming, 1985). Extrinsic factors, such as periphery-derived factors, as well as retrogradely transported factors, also play a role in the development of the PrV (Bates et al., 1982; Chiaia et al., 1991; Jhaveri et al., 1998). NMDA activity-dependent processes have been proposed to account for whisker-related pattern formation in the PrV (Li et al., 1994). However, genetic studies in mice suggest that NMDA-mediated activity probably plays a role in the consolidation of whisker-related pattern formation (Erzurumlu and Kind, 2001). Other than suspected N-methyl-D-aspartate (NMDA) NMDA-mediated neural activity and NGF (Henderson et al., 1994), no molecule has been found to account for the development of the PrV-based lemniscal pathway.

Received April 22, 2003; revised June 5, 2003; accepted June 17, 2003.

This work was supported by a National Institutes of Health (NIH) RO1 grant and a grant from McDonnell Center for Molecular and Cellular Neurobiology to Z-F.C., and NIH Grant PO1-DE07734 to M.F.J. We thank Dr. Thomas Woolsey for critical comments on this manuscript and discussion.

Correspondence should be addressed to Dr. Zhou-Feng Chen, Departments of Anesthesiology, Psychiatry, and Molecular Biology and Pharmacology, School of Medicine, Washington University, St. Louis, MO 63110. E-mail: chenz@morpheus.wustl.edu.

 0270-6474/03/237246-09$15.00/0

Drg11, a paired homeodomain transcription factor, is necessary for the assembly of the nociceptive circuitry in the dorsal spinal cord (Saito et al., 1995; Chen et al., 2001). In the present study, we set out to test the hypothesis that *Drg11* is essential for the development of the PrV-based lemniscal pathway.

Materials and Methods

Generation, maintenance, and genotyping of Drg11 mutant mice. $Drg11^{+/-}$ and $Drg11^{-/-}$ mice were generated and genotyped as described previously (Chen et al., 2001). The date when the plug is found is considered to be embryonic day (E) 0.5. The $Drg11^{+/-}$ mice are maintained in the mouse facility according to protocols approved by the Division of Comparative Medicine at the Washington University School of Medicine.

Histochemical staining. For cytochrome oxidase (CO) and NADPH stains, animals were perfused with 4% paraformaldehyde (PFA) at E18.5, E19.5, postnatal day (P) 1, P3, P7, or P14, and the brains were removed. After cryoprotection with 20% sucrose in 0.1 M PBS, pH 7.4, the brains were sectioned transversely at 50 μm or at 35 μm thickness tangentially (for viewing the barrels) in the S1 cortex, and then subjected to CO (Wong-Riley and Welt, 1980) or NADPH (Ding et al., 1993) staining. For CO staining, the sections were incubated with PBS containing 0.24 mg/ml cytochrome C (Sigma, St. Louis, MO; type III), 0.5 mg/ml DAB (Sigma), and 44 mg/ml sucrose (Sigma) for 2–4 hr at 37°C under gentle shaking. For NADPH staining, the sections were incubated with 0.1 M Tris-HCl buffer, pH 8.0, containing 1 mg/ml NADPH (Sigma; type I), 0.8 mg/ml nitroblue tetrozolium (Sigma), and 0.3% Triton X-100 for 2 hr at 37°C. The sections were mounted onto gelatin-coated glass slides and observed under an Olympus microscope (BX51).

For X-gal staining, embryos (E10.5–E13.5) were fixed with 4% PFA for 5 min, rinsed in PBS for 10 min, and incubated in PBS containing 0.15 M NaCl, 1 mM MgCl2, 0.003% Triton X-100, 0.001% potassium ferricyanide, 0.001% potassium ferrocyanide, and 1 mg/ml X-gal at 37°C for 1.5–2 hr. Some of embryos were sectioned at a thickness of 12 μm, and the sections were observed under the light microscope.

In situ *hybridization, immunocytochemistry, and cell counting.* For *in situ* hybridization, embryos (E10.5–E15.5, E18.5) were fixed in 4% PFA overnight and sunk in 15% sucrose. The embryos were frozen, sectioned, and kept on frosted slides. *In situ* hybridization was performed according to a procedure described previously (Birren et al., 1993). To detect expression of neomycin phosphotransferase II (Neo), immunocytochemistry was performed in both *Drg11* heterozygous and null mutants as described (Chen et al., 2001). The sections were sequentially incubated with rabbit anti-Neo antibody (Cortex Biochem, San Leandro, CA; 1:1000) in PBS containing 2% normal donkey serum and 0.3% Triton X-100 overnight, biotinylated donkey anti-rabbit (Jackson Immuno Research, West Grove, PA; 1:200) for 2 hr, and Cy3-congugated streptavidin (Molecular Probes, Eugene, OR; 1:1000) for 1 hr. After washing with PBS, the sections were counterstained with Hoechst (Acros Organics, Morris Plains, NJ) for localizing Neo-positive cells in the PrV. The number of Neo-positive cells in the PrV were counted in one series of sections from each embryo. These serial sections (four to five sections) covered the whole extent of the PrV. Data were indicated as mean ± SEM. Four $Drg11^{+/-}$ and three $Drg11^{-/-}$ embryos were used at each stage (E13.5, E14.5, E16.5), and Student's *t* test was used for statistical comparisons of the number of cells between $Drg11^{+-}$ and $Drg11^{-/-}$ embryos.

Terminal deoxynucleotidyl transferase-mediated biotinylated UTP nick end labeling (TUNEL) staining. After fixation with 4% PFA, the embryos (E14.5, E15.5, E16.5, E17.5, E18.5) were cryoprotected with 15% sucrose overnight, and serial 12-μm-thick sections were cut with a cryostat. The sections were directly mounted onto glass slides and then subjected to TUNEL examination (Gavrieli et al., 1992). After blocking endogenous peroxidases by incubation with 10% methanol and 3% H_2O_2 in PBS for 30 min at room temperature, the sections were incubated in a permeabilization solution (0.1% Triton X-100 in 0.1% sodium citrate) for 10 min. The sections were preincubated with terminal deoxynucleotidyl tranferase (TDT) buffer (1×; Promega, Madison, WI) for 5 min and then were incubated with the TDT buffer containing 0.5 mM TDT (Promega) and 40 μm biotin-dUTP (Roche, Indianapolis, IN) for 1 hr at 37°C. After being washed with PBS for 20 min, the sections were incubated with *Elite* ABC kit (Vector Laboratories, Burlingame, CA) for 30 min at 37°C, followed by an incubation with PBS containing 0.02% DAB and 0.003% H_2O_2 for 30 min for visualization. The positive cells (dying cells) were counted in the PrV, and comparisons between wild-type and $Drg11^{-/-}$ embryos were performed (for counting method, see above).

DiI and DiI/DiA labeling. Embryos at different stages and postnatal mouse brains were fixed with 4% PFA. For the study of projections from the whisker follicle to the PrV, a small amount of 1,1′-dioctadecyl-3,3,3′,3′-tetramethylindocarbocyanine perchlorate (DiI) or 4-[4-(dihexadecylamino)styryl]-*N*-methylpyridium iodide (DiA) (Molecular Probes) crystals were placed in the follicle(s). Tissues were kept in fixative at 37°C for 3–4 d (E12.5), 2 weeks (E13.5–E15.5), or 3–4 weeks (E16.5–E18.5). After the removal of the brainstems, they were vibratome sectioned transversely at 100 μm. Labeling was observed under an epifluorescent or laser confocal microscopy. The projections from the TG to the vibrissae follicles were examined by DiI labeling (E12.5–E15.5). DiI crystals were placed into the TG and kept between 5 d and 1 week. The projection from the PrV to the ventrobasal thalamus was studied at different stages as well (E14.5–E18.5). After the removal of the brains, they were cut in half at the level of the caudal pole of the PrV. DiI crystals were inserted into the PrV and stored for ~1 week (E15.5) or 2–3 weeks (E16.5–E18.5). Placement of DiI crystals into the ventrobasal thalamus was performed in a similar way, and the materials were kept for 5–7 d (E14.5, E15.5) or 1–2 weeks (E18.5, P3, P10) for tracer diffusion.

Results

Drg11 exhibits spatially restricted expression in the trigeminal brainstem complex

To determine the spatiotemporal pattern of *Drg11* expression in the developing trigeminal system, we examined the expression of *Drg11* in the trigeminal nuclei at different embryonic stages by *in situ* hybridization or X-gal staining. An IRES-tau-lacZ marker was previously introduced into the *Drg11* locus (Chen et al., 2001). Expression of the tau-lacZ gene was detected in the trigeminal pathway. A comparison of *Drg11* expression by *in situ* hybridization and by X-gal staining showed an identical staining pattern, indicating that the expression of the tau-lacZ gene mimics the expression of *Drg11*. The presumptive PrV cells first emerge from the ventricular zone of the ventral aspect of the hindbrain around E10.5 (Fig. 1*A*). One day later, the number of *Drg11*-expressing cells increased, and these cells migrated ventrolaterally toward the region that is adjacent to the TG (Fig. 1*B*). TG neurons also began to express *Drg11* at E11.5 (Fig. 1*B*). By E12.5, many early-born cells have reached the most ventrolateral part of the hindbrain and continue to express *Drg11* (Fig. 1*C*). By E15.5, *Drg11* expression appears to distribute uniformly in the PrV (Fig. 1*D*). *Drg11* is also expressed in the subnuclei oralis (SpVo) and SpVc at this stage (Fig. 1*F*) (data not shown for SpVo). However, in the SpVc, *Drg11* expression is notably absent in laminae III–IV (Fig. 1*F*), in which a whisker-related pattern develops (Henderson et al., 1992). *Drg11* expression is absent in SpVi (Fig. 1*E*), DCN, thalamus, or cortex (data not shown). Expression of *Drg11* in the PrV persists to postnatal stage (data not shown). Therefore, *Drg11* expression specifically marks a subset of PrV neurons from the time when they first emigrate from the ventricular zone of the ventral hindbrain and is also the earliest known gene to be expressed in PrV cells. Moreover, *Drg11* is the first identified gene whose expression distinguishes the PrV from the SpVi, raising the possibility that *Drg11* may have a subnuclear-specific role in trigeminal patterning.

Abnormal distribution of *Drg11*$^{-/-}$ cells and increased cell death in the PrV of *Drg11*$^{-/-}$ mice

To study the role of *Drg11* in the development of the PrV, we first stained the PrV of *Drg11*$^{+/-}$ and *Drg11*$^{-/-}$ embryos with X-gal at different stages. Up to E12.5, no difference in the staining pattern of migrating PrV cells was detected between *Drg11*$^{+/-}$ and *Drg11*$^{-/-}$ embryos (data not shown). Over the next few days, presumptive PrV cells continued their ventrolateral migration, as described previously (al-Ghoul and Miller, 1993). Beginning at E14.5, the PrV began to exhibit its characteristic half-moon shape in transverse sections, as indicated by clusters of densely populated cells in the most ventrolateral hindbrain. Morphological differences in the PrV of *Drg11*$^{-/-}$ and wild-type controls detected by Nissl staining were not seen up to E16.5 (data not shown).

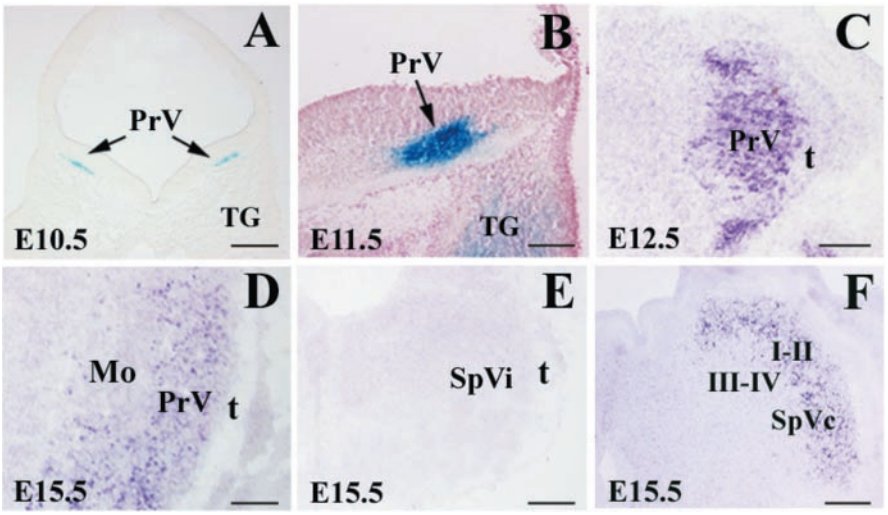

Figure 1. Expression of *Drg11* in the PrV, SpVi, and SpVc. *Drg11* expression detected by X-gal staining (*A*, *B*) and *in situ* hybridization (*C–F*) in transverse sections through the hindbrain. *A*, At E10.5, *Drg11* is expressed in presumptive PrV cells that begin to emerge from the ventricular zone of the ventral hindbrain (arrow). *B*, At E11.5, *Drg11* expression increases as more PrV cells emerge from the ventricular zone (arrow). *C*, At E12.5, *Drg11* expression is concentrated in the presumptive PrV region. *D*, At E15.5, *Drg11* expression encompasses PrV. *E*, No *Drg11* expression is detected in the SpVi. *F*, Drg11 is expressed in laminae I–II but not in III–IV of the SpVc. Mo, Motor trigeminal nucleus, t: spinal trigeminal tract. Scale bars, 100 μm.

To assess the distribution of *Drg11*$^{-/-}$ cells in *Drg11*$^{-/-}$ mutants, *Drg11*$^{-/-}$ cells in the PrV were monitored by the use of anti-Neo immunocytochemistry (Chen et al., 2001). Between E11.5 and E13.5, *neo* expression in *Drg11*$^{-/-}$ mutants was homogenous in the PrV, resembling its expression in *Drg11*$^{+/-}$ embryos (data not shown). At E14.5, neo expression in the PrV of the *Drg11*$^{+/-}$ embryo maintained its widespread expression throughout the PrV (Fig. 2*A*,*C*). However, in *Drg11*$^{-/-}$ mutants, an abnormal distribution of *Drg11*$^{-/-}$ cells was detected: few *neo*$^{+}$ cells were found in the most ventrolateral region of the PrV, despite the presence of numerous PrV cells in this region (Fig. 2*B*,*D*). Counting of *neo*$^{+}$ cells in the PrV revealed no significant difference between *Drg11*$^{+/-}$ and *Drg11*$^{-/-}$ embryos (Fig. 2*E*). At E16.5, an aberrant aggregation of *Drg11*$^{-/-}$/ *neo*$^{+}$ cells became more prominent in the PrV (Fig. 2*F*,*G*). Similarly, no significant difference in the number of *neo*$^{+}$ cells in the PrV was found between *Drg11*$^{+/-}$ and *Drg11*$^{-/-}$ embryos at this stage (Fig. 2*H*). By E18.5, the PrV in the mutant was smaller than the control (data not shown).

To ascertain whether an abnormally increased cell death occurs in the PrV of *Drg11*$^{-/-}$ embryos, TUNEL staining was performed. Whereas TUNEL staining was normal before E18.5 (data not shown), the number of TUNEL^{+} cells in the mutant PrV was significantly increased in the mutants at E18.5 (Fig. 2*I–K*). By contrast, no abnormal cell death was noted in the SpVi and in the deep laminae of the SpVc of *Drg11*$^{-/-}$ embryos at this stage (data not shown). Therefore, the earliest stage when we could identify a morphological abnormality in the PrV is at E14.5, and abnormal PrV cell death was first detected at E18.5.

Loss of *Ebf1* expression in the PrV of *Drg11*$^{-/-}$ mice

To determine whether *Drg11* is required for expression of other transcription factors in PrV cells, a panel of molecular markers were examined in the PrV of *Drg11*$^{-/-}$ embryos. Early B-cell factors (Ebf)/olfactory factor 1 are members of the helix-loop-helix transcription factors and play multiple roles in a variety of developmental processes (Dubois and Vincent, 2001). Three members of the *Ebf* family, *Ebf1*, *Ebf2*, and *Ebf3*, are expressed in the developing PrV cells (Wang and Reed, 1993; Wang et al., 1997). *In situ* hybridization studies indicated that, up to E13.5, expression of these markers in the PrV of *Drg11*$^{-/-}$ embryos was normal (data not shown). However, beginning at E14.5, expression of *Ebf1* was abolished in the PrV of *Drg11*$^{-/-}$ embryos (Fig. 3*A*,*B*), whereas expression patterns of *Ebf2* and *Ebf3* were unaltered (Fig. 3*C*--*F*). Thus, *Ebf1* appears to act downstream of *Drg11*. *Rnx* is a member of the *Tlx* homeodomain-containing gene family and is expressed in many brainstem nuclei, including the PrV, during development (Logan et al., 1998; Qian et al., 2002). In the PrV of *Rnx* mutants, the initiation of *Drg11* expression is normal, however, its expression is absent at a later stage, suggesting that *Rnx* is required for maintaining *Drg11* expression in the developing PrV (Qian et al., 2002). We found that in the PrV of the *Drg11* mutant, *Rnx* expression was not affected (Fig. 3*G*,*I*). Among these markers examined, *Ebf1*, *Ebf2*, and *Rnx* were also expressed in SpVi. However, their expression was not changed in the SpVi of *Drg11*$^{-/-}$ mice (data not shown). These results suggest that *Drg11* acts downstream of *Rnx* and is required for maintaining expression of *Ebf1* in the PrV.

Abnormal central projections of TG afferents in *Drg11*$^{-/-}$ mice

To assess the central projections of TG afferents, rows of vibrissal follicles of *Drg11*$^{-/-}$ embryos were labeled with DiI. At E11.5, afferents in *Drg11*$^{-/-}$ embryos have reached the brainstem on a normal time schedule (data not shown). On arriving at the brainstem, TG afferents bifurcate: the rostral branches enter the PrV, whereas the caudal branches innervate the trigeminal spinal nuclei. By E14.5, both wild-type and mutant TG afferents from the b2 vibrissae follicle penetrated the PrV, and no major difference in the projection pattern was found between wild-type and *Drg11*$^{-/-}$ mice (Fig. 4*A*,*B*). One day later, afferents from the c2 and d2 vibrissal follicles grow toward the more inner medial region of the PrV (Fig. 4*C*,*D*). The density and morphology of DiI-labeled collaterals in the mutant PrV were indistinguishable from those in the wild-type controls. By E16.5, in wild-type embryos, DiI-labeled fibers from the b2 and b3 follicles were much more abundant and have reached the inner portion of the PrV (Fig. 4*E*). However, in the mutants, the projections of TG affer-

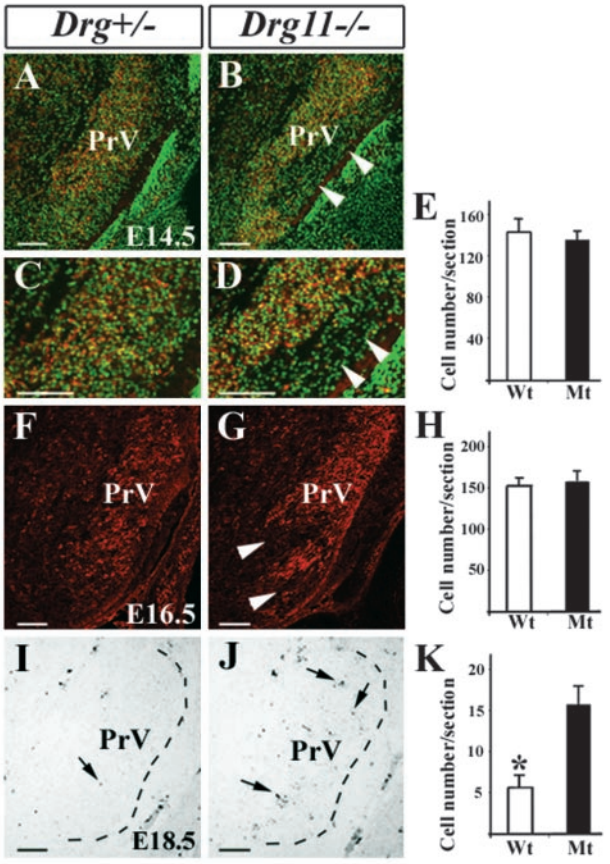

Figure 2. Immunocytochemical staining of *neo*$^{+}$ cells and TUNEL studies of the PrV in wild-type and *Drg11*$^{-/-}$ mice. *A*, *B*, Neo staining (red) and Hoechst countstaining (green) of the PrV in wild-type (*A*, *C*) and *Drg11* (*B*, *D*) mutants at E14.5. Arrowheads indicate the region where few *Drg11*$^{-/-}$/*neo*$^{+}$ cells were found. *C*,*D*, Higher magnification of *A*, *B*. *E*, Comparison of the number of *Drg11*$^{+/-}$ and *Drg11*$^{-/-}$ cells in the PrV at E14.5. Neo^{+} cells in *Drg11*$^{+/-}$ embryos at E14.5, 143.7 ± 8.1; in *Drg11*$^{-/-}$ embryos, 135.4 ± 5.2; $p = 0.061$ ($p > 0.05$). *F*, *G*, *Neo* staining (red) in the PrV of the wild-type embryos (*F*) and the mutant (*G*) at E16.5, Note that in the most ventral aspect (arrowheads) of the mutant PrV, *Drg11*$^{-/-}$ cells appear to avoid certain regions. *H*, Comparison of the number of *Drg11*$^{+/-}$ and *Drg11*$^{-/-}$ cells in the PrV at E14.5. Neo^{+} cells in *Drg11*$^{+/-}$ embryos at E16.5, 153.6 ± 8.7; in *Drg11*$^{-/-}$ embryos, 160.3 ± 13.7; $p = 0.72$ ($p > 0.05$). *I*, *J*, At E18.5, TUNEL studies revealed increased cell death in the mutant PrV (*J*, arrow) compared with the wild-type PrV (*I*, arrows). *K*, Comparison of the number of apoptotic cells in the PrV between wild-type and *Drg11* mutant embryos at E18.5. The average number of apoptotic cells in the PrV. Wild-type embryo, 5.3 ± 1.4; *Drg11* mutant, 15.0 ± 2.3; $p = 0.015$ ($p < 0.05$). Scale bars, 100 μm.

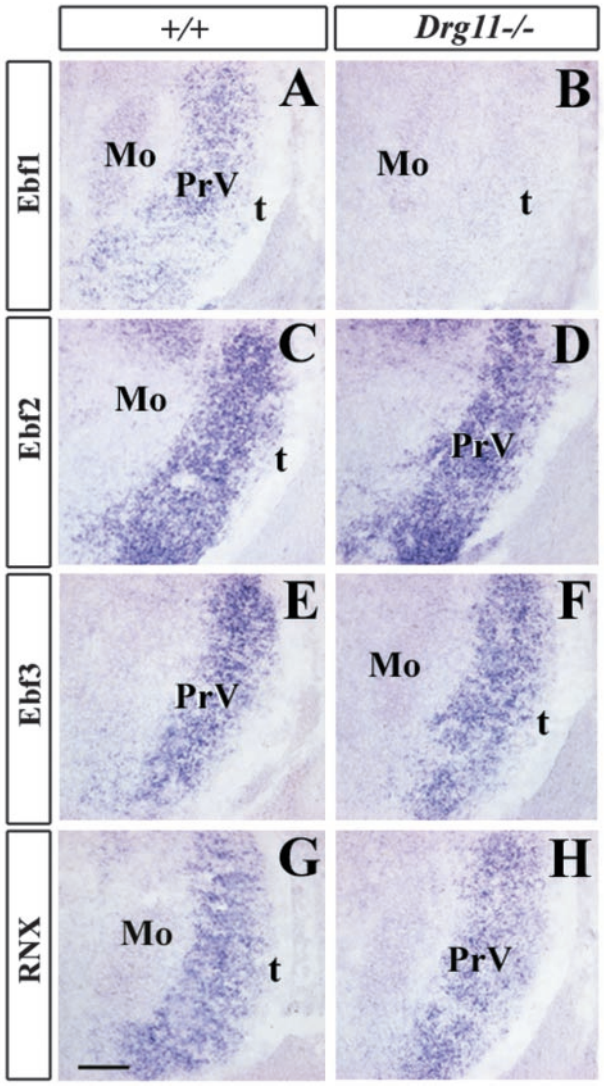

Figure 3. Expression of molecular markers in the PrV detected by *in situ* hybridization. Transverse sections of the E14.5 PrV of wild-type (*A*, *C*, *E*, *G*) and *Drg11*$^{-/-}$ (*B*, *D*, *F*, *H*) embryos. *A*, *B*, Ebf1 expression is detected in the wild type (*A*), but not in the mutant (*B*). No significant changes are found in the expression pattern of *Ebf2* (*C*,*D*), *Ebf3* (*E*, *F*), and *Rnx* (*G*,*H*) between the wild-type and mutant PrV at E14.5. Scale bar, 100 μm.

ents were abnormal (Fig. 4*F*). Most fibers had unusual orientations for the b row axons in having more ventromedial trajectories in the PrV than normal controls. A few fibers had aberrant dorsolateral trajectories (Fig. 4*F*). At E18.5, wild-type fibers from the c2 vibrissae follicle gave rise to collaterals that aggregated into a single cluster that is confined to the ventromedial region of the PrV (Fig. 4*G*). In the mutant, consistent with the aforementioned E16.5 projection pattern, DiI-labeled fibers from the c2 follicle did not enter the inner medial region of the PrV (Fig. 4*H*). Rather, they were confined to a ventrolateral position (Fig. 4*H*). These aberrant projections suggest that there are pathfinding errors for immature trigeminal afferents in the mutants. In contrast, mutant TG afferents appeared to innervate the SpVi in a normal manner at this stage (Fig. 4*I*, *J*).

We also assessed the projections of TG afferents to the vibrissae follicles by labeling of TG cells with DiI crystals. Between E12.5 and E14.5, TG axons appeared to normally grow toward the periphery in *Drg11*$^{-/-}$ embryos (data not shown). By E15.5, DiI tracing revealed mutant afferents encircling individual follicles as in wild-type afferents (Fig. 4*K*, *L*). The density of TG afferents enveloping vibrissal follicles also appeared similar between wild-type and *Drg11*$^{-/-}$ embryos. In addition, X-gal staining also failed to distinguish wild-type and mutant projections (data not shown). These results suggest that the peripheral projections of TG afferents are grossly normal in *Drg11*$^{-/-}$ embryos.

Site-specific deficits in somatotopic pattern formation in *Drg11*$^{-/-}$ mice

The abnormal development of the PrV promoted examination of whisker-related pattern formation in *Drg11*$^{-/-}$ mice by CO staining. Histochemical staining of CO activity in somata, dendrites, and axonal terminals in different subcortical and cortical regions identifies individual cell aggregates, or patches, each corresponding to single whiskers in rodents (Wong-Riley and Welt, 1980; Killackey et al., 1990). In wild-type mice, five rows

of CO-stained patches corresponding to five rows of whiskers were present in the PrV, SpVi, SpVc (barrelettes), VPm (barreloids), and S1 cortex (barrels) (Fig. 5*A*,*C*,*E*,*G*,*I*). No such patterned CO-stained patches were discernable in the PrV, VPm, or S1 cortex of *Drg11*$^{-/-}$ mice (Fig. 5*B*,*D*,*F*). However, robust patterns were detected in the SpVi and SpVc of *Drg11*$^{-/-}$ mice (Fig. 5*H*,*J*). Whereas robust whisker-related patterns were detected in the SpVi and SpVc, the patterns appeared to be incomplete in some cases, and individual patches were smaller than those in the wild-type controls (Fig. 5*H*,*J*). This may be a consequence of pervasive cell death in the PrV, which is a major target of the patterned SpVi and SpVc cells (Jacquin et al., 1990).

The lack of patterning in specific portions of the barrel neuraxis, as revealed by CO staining, could also be because of a lack of CO activity or a metabolic abnormality in CO synthesis, as opposed to a lack of neuronal patterning. To assess this possibility, we used an alternative staining method: expression of NADPH (Mitrovic and Schachner, 1996; Pereira et al., 2000), a synthase for nitric oxide that stains neuropil in the PrV and S1 cortex and is normally equivalent to that revealed by CO (Mitrovic and Schachner, 1996; Pereira et al., 2000). Whereas distinct patterns of NADPH staining were detected in the PrV, VPm, and layer IV of the S1 cortex of wild-type mice, no such patterns were observed in the mutants (Fig. 5*M–P*) (data not shown). Similarly, somatotopic NADPH patterns were found in the SpVi and SpVc of both wild-type and *Drg11*$^{-/-}$ mutants (data not shown). Thus, whisker-related patterns fail to form specifically in the PrV-based lemniscal pathway in *Drg11*$^{-/-}$ mice.

To assess whether lack of CO and NADPH patterning was because of a failure in either pattern formation or pattern maintenance in *Drg11*$^{-/-}$ mutants, we performed CO and NADPH histochemistry from the earliest stage at which patterns are normally visible. In wild-type controls, the patterns first emerge in the brainstem at E18.5, as detected by CO staining, in the VPm at P2 and in the S1 cortex at P3 (Ma, 1993). No patterns were detected in the PrV, VPm, and S1 cortex of *Drg11*$^{-/-}$ mice at any stages examined (data not shown). Therefore, the lack of patterns in *Drg11*$^{-/-}$ mice is because of a failure in pattern formation, rather than in its maintenance.

We next assessed pattern formation in the DCN-based lemniscal pathway. In wild-type mice, forepaw and hindpaw digits were recognizable as discrete patches in the VPl and S1 cortex by CO staining (Fig. 5*C*,*E*) (data not shown). Forepaw and hindpaw digit patches were also identified in the VPl thalamus and S1 cortex of *Drg11*$^{-/-}$ mice (Fig. 2*D*,*F*) (data not shown). The digit patterns were also present in the gracile nucleus and cuneate nucleus of the mutant DCN (Fig. 5*K*,*L*). Thus, both hindpaw and forepaw digit patterns developed in *Drg11*$^{-/-}$ mice.

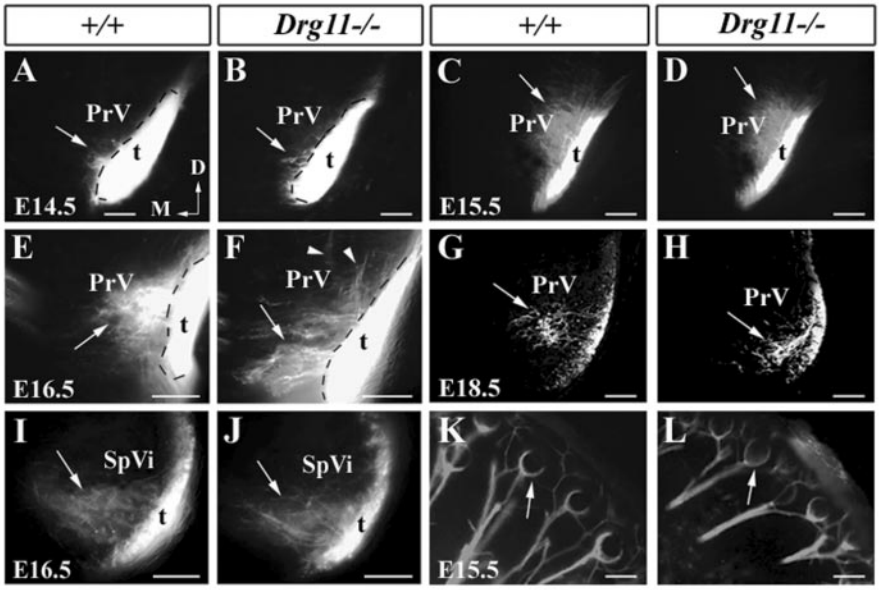

Figure 4. Central and peripheral projections of TG afferents in wild-type and *Drg11* mutant embryos as revealed by DiI staining. *A*, *B*, At E14.5, both wild-type (*A*) and mutant (*B*) TG afferents enter the PrV (arrows). Note that DiI crystals were applied to the b2 vibrissal follicle. *C*,*D*, At E15.5, more DiI-labeled axons are observed within the wild-type (*C*) and mutant (*D*) PrV. Most afferents have a dorsomedial trajectory (*C*,*D*, arrows). No major abnormality is noted in the mutant (*D*). Note that DiI crystals were applied to the c2 and d2 vibrissal follicles. *E*, *F*, At E16.5, DiI-labeled wild-type afferents further reach the inner region of the PrV with a dorsomedial trajectory (*E*, arrow). The mutant afferents display ventromedial trajectories (*F*, arrow). A few afferent fibers grow aberrantly in a dorsolateral direction (*F*, arrowheads). Note that DiI crystals were applied in the b2 and b3 vibrissal follicles. *G*,*H*, At E18.5, TG afferents become clustered (*G*, arrow) in the inner region of the PrV in wild-type mice (*G*, arrow). By contrast, mutant afferent clusters are located in more ventrolateral regions (*H*, arrow). Note that DiI crystals were placed in the c2 vibrissal follicle. These images were obtained through the use of a laser confocal microscope. *I*, *J*, No difference in the projection patterns of TG afferents is found between the SpVi of wild-type (*I*, arrow) and mutant (*J*, arrow). Note that DiI crystals were placed in the b2 and b3 follicles. *K*, *L*, DiI tracing of TG afferents to the vibrissal follicles of E15.5 wild-type (*K*, arrow) and mutant (*L*, arrow). Note that DiI-labeled fibers surround the base of the follicles and exhibit a circumferential profile (*K*, *L*, arrows). Scale bars, 100 μm.

Delayed thalamic projections of PrV cells in *Drg11*$^{-/-}$ mice

The abnormal distribution of PrV cells, the loss of *Ebf1* expression, and increased TUNEL staining indicated that the development of the PrV is severely impaired in *Drg11*$^{-/-}$ mice. Do PrV cells project normally to the contralateral VPm in *Drg11*$^{-/-}$ embryos? To address this question, PrV axons were anterogradely labeled with DiI. To exclude the possibility that labeling may spuriously include the SpVi, the caudal brainstem at the level of the caudal pole of the PrV was removed before applying DiI to the PrV. At E17.5, PrV axons have reached the VPm and outline the contour of the VPm (Fig. 6*A*). However, at this stage, PrV axons labeled by DiI were not detected in the VPm of *Drg11*$^{-/-}$ embryos (Fig. 6*B*). By E19.5, the mutant PrV axons have reached the VPm, but the intensity and areal expanse of labeling was much less (Fig. 6*C*,*D*), suggesting that the projections of PrV axons were greatly reduced in number and area. We next examined the morphology of the VPm by Nissl staining. No difference in the gross morphology of the VPm between *Drg11*$^{-/-}$ and wild-type embryos was found up to E18.5 (data not shown). These data demonstrated a delayed projection of PrV efferents to the VPm and a resultant projection that is reduced in areal extent. Given that *Drg11* is not expressed in the VPm, the projection abnormalities of PrV cells must reflect an abnormal development of PrV cells, rather than a target field defect.

Lack of a barrel-like distribution of TCAs in *Drg11*$^{-/-}$ mice

To determine whether TCAs project to the S1 cortex and form whisker-like patterns in *Drg11*$^{-/-}$ mice, the projections of TCAs to the cortex were examined by applying DiI crystals to the ven-

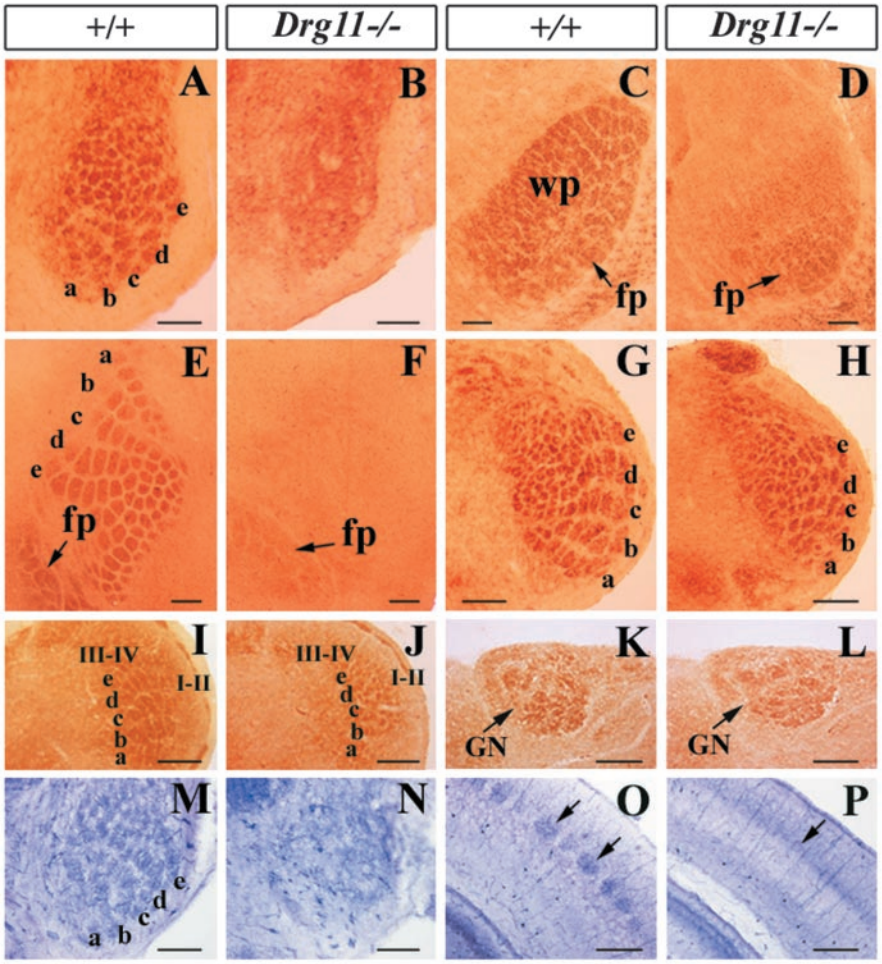

Figure 5. Somatotopic patterns in *Drg11*$^{-/-}$ and wild-type mice. *A–J*, CO staining of the whisker-like patterns in the PrV (*A*, *B*), VPm (*C*,*D*), S1 cortex (*E*,*F*, tangential section), SpVi (*G*,*H*), and SpVc (*I*,*J*). Note the absence of CO-stained patterns in the mutant PrV (*B*), VPm (*D*), and S1 cortex (*F*) but the presence of the patterns in the SpVi (*H*) and SpVc (*J*) of *Drg11*$^{-/-}$ mice. In the VPl thalamus and S1 cortex of the mutant, forepaw digit patterns were present (*C*,*F*, arrows). *M*, *O*, NADPH expression exhibits whisker-like patterns in the PrV (*M*) and S1 cortex (*O*) of wild-type mice and their absence in *Drg11*$^{-/-}$ mice (*N*, *P*). *K*, *L*, CO staining of the hindpaw digit patterns in the gracile nucleus (GN) of wild-type (*K*) mice and in the mutant (*L*). I–II, laminae I and II of the SpVc; III–IV, laminae III and IV of the SpVc; wp, whiskerpad representation; fp, forepaw representation. Scale bars, 100 μm.

trobasal thalamus and anterogradely labeling their projections during development. TCAs originating in the ventrobasal thalamus grow ventrally, project through the internal capsule, and then turn dorsally to reach the neocortex before they branch off to the nascent layer IV of the S1 cortex (Bernardo and Woolsey, 1987; Braisted et al., 1999). TCAs first arrive at the cortex on E14.5 in mouse but do not branch in layer IV until after birth (Senft and Woolsey, 1991; Agmon et al., 1993; Cohen-Tannoudji et al., 1994). At E15.5, labeled TCAs were clearly present in the cortex of wild-type mice with a few branching toward nascent layer IV (Fig. 6*E*). TCAs behaved similarly in *Drg11*$^{-/-}$ embryos (Fig. 6*F*).

TCAs branch to layer IV of the S1 cortex initially in a uniform distribution pattern and later are sculpted into whisker-related patches (Rebsam et al., 2002). To determine whether TCAs form a barrel-like pattern in layer IV of S1 cortex in *Drg11*$^{-/-}$ mice, DiI anterograde labeling experiments were performed in postnatal mice. At P10, patches corresponding to individual barrels were present in layer IV of the wild-type cortex. In contrast, DiI-labeled fibers, although of similar labeling intensity, did not form barrel-like patches in the mutant. Rather, DiI-labeled TCAs were distributed uniformly in layer IV of the S1 cortex (Fig. 6*G*,*H*).

Normal gross topography of TG afferents in *Drg11*$^{-/-}$ mice

Somatotopic pattern formation in subcortical regions requires topographic projections of primary afferents. Although patterns first develop during the late embryonic stages or early postnatal periods, the topography of afferent projections is established much earlier (Erzurumlu and Jhaveri, 1992). A lack of whisker-related patterns in *Drg11*$^{-/-}$ mice prompted examination of a potentially altered topography of TG afferents. DiI and DiA crystals were applied to distinct regions of the whiskerpad of E12.5 embryos, and their projections were examined in TG neurons and the brainstem. Two labeled clusters were routinely distinguishable in TG neurons (Fig. 7*A*,*B*) and in their projections within the brainstem nuclei (Fig. 7*C*,*D*). DiI was then applied into the b2 and d2 whisker follicles of E15.5 embryos. In the wild-type and mutant PrV, two widely separated patches of DiI-labeled terminal clusters were clearly present (Fig. 7*E*,*F*). Similarly, two distinct patches were also observed in the SpVi of both wild-type and *Drg11*$^{-/-}$ embryos (Fig. 7*G*,*H*). These results demonstrated that there was a grossly normal topography of TG projections in the *Drg11*$^{-/-}$ mice.

Discussion

The molecular mechanisms underlying the development of the PrV-based lemniscal pathway are poorly understood. In this study, we have characterized the development of the PrV in *Drg11*$^{-/-}$ mice and found that in the absence of *Drg11*, *Drg11*$^{-/-}$ cells distribute abnormally and PrV efferents project to VPm aberrantly, followed by an increase of abnormal cell death in the PrV. Moreover, the projections of TG afferents to the PrV are aberrant. As a result, whisker-related patterns fail to form in the PrV, VPm, and S1 cortex. By contrast, such patterns form in the SpVi, SpVc, DCN, and associated VPl and limb cortex. Together, our results demonstrate that *Drg11* is essential for the proper development of the PrV cells and is the first identified molecule that distinguishes the PrV-based lemniscal pathway from the SpVi-based paralemniscal pathway.

Drg11 is required for the development of the PrV

Drg11 is the earliest known marker that marks the birth of PrV cells (Fig. 1). Insofar as the onset of *Drg11* expression coincides with the migration of PrV cells, *Drg11* could be involved in migration. By the use of tau-lacZ as a marker, no notable difference in the migratory behavior of PrV cells was observed in the absence of *Drg11* function between E11.5 and E13.5. Nevertheless, one cannot completely rule out the possibility that a subset of the

mutant PrV cells may migrate aberrantly. Once the cells have reached their destination, and begin to form the PrV, several prominent molecular and cellular abnormalities occur in *Drg11*$^{-/-}$ embryos: an abnormal distribution of *Drg11*$^{-/-}$ cells, the loss of *Ebf1* expression, aberrant thalamic projections, and abnormal cell death (Figs. 2, 3, 6). In addition, aberrant projections of TG afferents within the PrV are also found (Fig. 4). The timing of each defect that occurs is significant because it permits reasonable interpretation of the primary locus of the action of the mutation. The latter is believed to be PrV morphogenesis in light of the following: the first sign of abnormal distribution of the PrV cells and loss of *Ebf1* gene expression are detected at E14.5, abnormal projections of TG afferents to the PrV at E16.5, a delayed and reduced thalamic projections at E17.5, followed by an increased cell death in the PrV at E18.5. The finding that there is a segregation of *Drg11*$^{-/-}$ cells from non-*Drg11*-expressing cells in the outermost PrV, as reflected in *neo* expression pattern, strongly suggests that *Drg11* is involved in the morphogenesis of the PrV cells (Fig. 2). This phenotype is reminiscent of the abnormal dorsal horn morphology detected in *Drg11*$^{-/-}$ embryos, suggesting that *Drg11* may control the similar cellular events in both regions (Chen et al., 2001). It is interesting to note that the abnormal distribution of PrV cells is most prominent in the ventral aspect of the PrV, in which the whisker-related patterns are detected a few days later (Fig. 2). By contrast to this early morphogenetic deficit, abnormal cell death in the PrV ensues only 4 d later (E18.5). Thus, it is less likely that this abnormal cell death in the PrV is a primary defect.

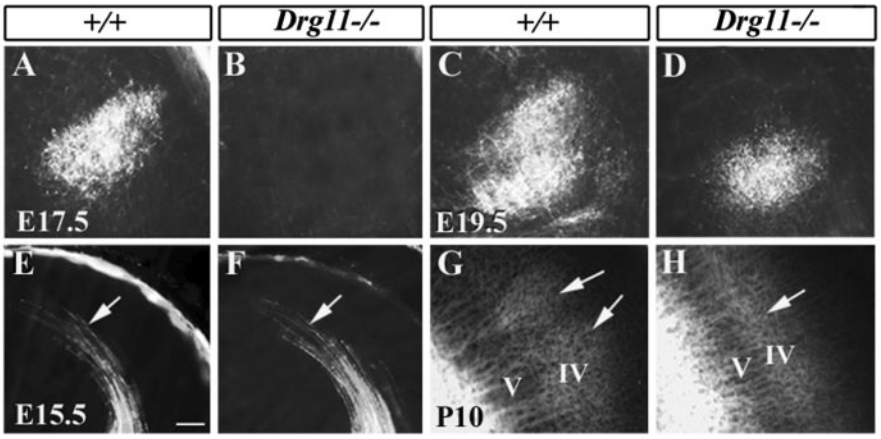

Figure 6. Projections of PrV efferents and TCAs revealed by DiI tracing. *A–D*, DiI tracing of PrV projections in the VPm. *A*, *B*, Whereas PrV efferents are present in the E17.5 wild-type VPm (*A*), no DiI-labeled axons are present in the mutant VPm (*B*). *C*,*D*, At E19.5, DiI-labeled PrV efferents are found in both the wild-type (*C*) and mutant (*D*) VPm, but the extent of DiI labeling in the mutant is much reduced (*D*). *E–H*, DiI tracing of TCAs in the S1 cortex. *E*, *F*, At E15.5, TCAs of wild-type and mutants labeled by DiI are found in the S1 cortex. Arrows point to the growth cones of TCAs that arrive at S1 cortex. No major difference is found in the projection patterns. *G*,*H*, The projection of TCAs in layer IV of the cortex at P10. In wild-type mice (*G*), DiI-labeled axons aggregate to form individual patches corresponding to single barrels (*G*, arrows), but in the mutant (*H*), DiI-labeled axons are distributed evenly. Scale bar, 100 μm.

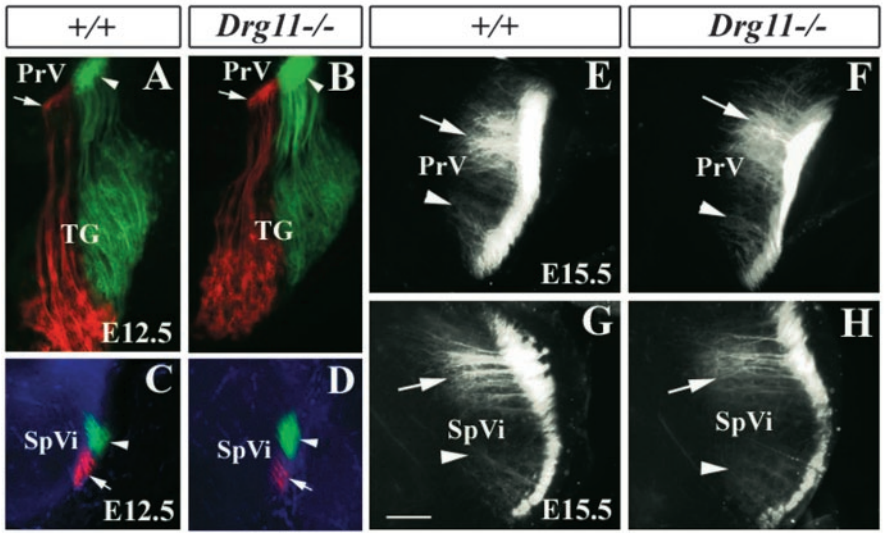

Figure 7. Topographic organization of the TG projections revealed by DiI and DiA double labeling. *A–D*, DiI and DiA were applied in the dorsal and ventral vibrissae follicles of wild-type (*A*, *C*) and mutant (*B*, *D*) embryos, respectively, at E12.5. DiI-labeled (red; arrows) and DiA-labeled (green; arrowheads) axons are segregated in the TG (*A*, *B*), PrV (*A*, *B*), and SpVi (*C*,*D*). No major difference between the wild type and mutant is noted. *E*, *H*, DiI crystals were applied to distinct vibrissae follicles of wild-type (*E*, *G*) and mutant (*F*, *H*) embryos, respectively, at E15.5. Two well separated foci of DiI-labeled afferents mark distinct clusters of TG afferents in the PrV (*E*, *F*, arrowheads) and SpVi (*G*,*H*, arrowheads). Note the equivalent locations and densities of labeled afferents in the wild type and mutants. Scale bar, 100 μm.

Because *Drg11* is expressed in both the TG and PrV, one important issue to consider is whether the abnormal projections of TG primary afferents reflect a primary requirement for *Drg11* in the TG or PrV, or both. Several lines of evidence support the notion that a lack of whisker-related patterning primarily reflects the defects in the PrV, rather than a defect in the TG. First, intra-axonal labeling of hundreds of TG afferents revealed that the same axons of TG neurons always innervate both the PrV and SpVi (Hayashi, 1980; Shortland et al., 1996). If the primary defect of the *Drg11* mutation lies in these TG neurons, the aberrant projections of TG afferents would also be reflected in the SpVi. However, in *Drg11*$^{-/-}$ mice, projections of TG afferents in the SpVi and subsequent pattern formation there appeared normal (Figs. 4, 5). Second, the PrV-specific expression of *Drg11* in normal development is well correlated with the PrV-specific deficits in the *Drg11* mutants. Finally, the timing of the abnormal distribution of cells and the altered molecular expression profile in the PrV precedes the projection abnormalities of TG afferents. Taken together, the factors causing the aberrant projection of TG afferents in their central target of the *Drg11* mutants are most likely to be intrinsic to the PrV cells.

A previous study showed that a homeodomain transcription factor, *Rnx*, is required for the maintenance of *Drg11* expression (Qian et al., 2002). The present study indicates that *Drg11* is required for the maintenance of *Ebf1* expression (Fig. 3). Examination of the PrV of *Ebf1*$^{-/-}$ mice did not reveal any gross deficits, possibly reflecting a functional compensation by *Ebf2* and *Ebf3* (Y-Q. Ding and Z-F. Chen, unpublished data). However,

these studies begin to identify a genetic cascade that is essential for the proper development of the PrV.

Drg11-dependent formation of PrV-based lemniscal pathway

In *Drg11*$^{-/-}$ mice, somatotopic patterning in the PrV, VPm, and S1 cortex is disrupted, as demonstrated by histochemical and Nissl staining and DiI labeling (Fig. 5) (data not shown). Whereas abnormal morphogenesis of PrV cells and central projection deficits in the PrV are first detected in *Drg11*$^{-/-}$ mice between E14.5 and E16.5, abnormal patterning is only apparent a few days later, when patterns are first visible normally (Chiaia et al., 1992; Ma, 1993). Because an abnormal distribution of PrV cells precedes the projection deficit of the TG afferents, normal morphogenesis of PrV cells may be essential for the normal projections of TG afferents in the PrV. The observation that *Drg11* is not expressed in the thalamus and cerebral cortex indicates that the failure of pattern formation in the VPm and S1 cortex must be a consequence of the earlier deficit in the PrV, given the central role for the PrV in higher-order somatotopic patterning (Killackey and Fleming, 1985). The early embryonic phenotype in the PrV suggests that altered pattern formation might be an indirect effect of abnormal morphogenesis and cell death in PrV cells. In this regard, the role of *Drg11* in pattern formation may differ from NMDA receptors, which appear to have a direct role in the consolidation and refinement of somatotopic map (Li et al., 1994; Kutsuwada et al., 1996; Iwasato et al., 1997). Insofar as *Drg11* is also expressed in the postnatal PrV, analysis of the effects of postnatal conditional knock-out of the gene would be a useful test of the hypothesis that *Drg11* also has a direct role in somatosensory pattern formation exclusive of its role in embryonic PrV development. Nevertheless, our results extend previous study (Killackey and Fleming, 1985) to a specific molecular deficit in the PrV that interrupts whisker-related pattern formation in the thalamus and barrel cortex.

The delay in arrival of PrV-thalamic projections must reflect an intrinsic impairment of PrV cells because *Drg11* is not expressed in the VPm (Fig. 6). Furthermore, the reduced areal expanse of PrV-thalamic projections at E19.5 may simply reflect the reduced number of PrV cells caused by early cell death (Fig. 2) (data not shown). Despite the seeming absence of PrV inputs to the thalamus before E19.5, TCAs do navigate to layer IV of the S1 cortex without delay (Fig. 6). This is consistent with previous observations that the navigation of TCAs toward the cortex is a target- and environment-dependent process and does not require PrV-relayed, whisker-related inputs (Molnar and Blakemore, 1995; Braisted et al., 1999, 2000). Nevertheless, our studies render further evidence that the segregation of TCAs into a barrel-like pattern is a presynaptic signal-dependent process (Cases et al., 1996; Rebsam et al., 2002).

Drg11: a key molecular determinant that distinguishes the formation of the PrV-based leminscal pathway from SpVi- and SpVc-based pathway

An important finding in the present study is that the PrV-based whisker-related lemniscal and cortical patterns fail to form in *Drg11*$^{-/-}$ mice, whereas somatotopic patterns form in the SpVi-based paralemniscal pathway and in the SpVc. Moreover, forepaw and hindpaw digit patterning also develops in the DCN, VPl, and S1 cortex (Fig. 5). Therefore, the patterning effect in *Drg11*$^{-/-}$ mice displays an unprecedented specificity.

The SpVi-based lemniscal and the SpVi-based paralemniscal pathways are parallel pathways that take origin in patterned nuclei. However, their thalamic projection patterns are different: the PrV cells terminate preferentially in the VPm, whereas the SpVi thalamic-projecting cells terminate preferentially in the posterior nucleus of the thalamus (Williams et al., 1994). In addition, SpVi cells also project to the PrV (Jacquin et al., 1990). Thus, the PrV and SpVi play different roles in mediating whisker-related information transmission. The molecular mechanism that dictates the formation of these two pathways is not known. In the SpVc, somatotopic patterning is observed only in laminae III–IV, but not in laminae I–II (Fig. 1). Interestingly, *Drg11* expression is notably restricted to laminae I–II. Therefore, whereas a somatotopic pattern is present in three trigeminal sunuclei, *Drg11* is uniquely expressed in the PrV. Our study strongly argues that *Drg11* is a key determinant of a molecular machinery that distinguishes the formation of the PrV-based lemniscal pathway from that of the DCN-based lemniscal pathway and the SpVi-based paralemniscal pathway. Although it is not clear to what extent the molecular machinery among the PrV, SpVi, and SpVc differ, further unraveling of the molecular cascade in which *Drg11* acts may be one of the first steps to address this question.

References

Agmon A, Yang LT, O'Dowd DK, Jones EG (1993) Organized growth of thalamocortical axons from the deep tier of terminations into layer IV of developing mouse barrel cortex. J Neurosci 13:5365–5382.

al-Ghoul WM, Miller MW (1993) Orderly migration of neurons to the principal sensory nucleus of the trigeminal nerve of the rat. J Comp Neurol 330:464–475.

Bates CA, Killackey HP (1985) The organization of the neonatal rat's brainstem trigeminal complex and its role in the formation of central trigeminal patterns. J Comp Neurol 240:265–287.

Bates CA, Erzurumlu RS, Killackey HP (1982) Central correlates of peripheral pattern alterations in the trigeminal system of the rat. III. Neurons of the principal sensory nucleus. Brain Res 281:108–113.

Bernardo KL, Woolsey TA (1987) Axonal trajectories between mouse somatosensory thalamus and cortex. J Comp Neurol 258:542–564.

Birren SJ, Lo L, Anderson DJ (1993) Sympathetic neuroblasts undergo a developmental switch in trophic dependence. Development 119:597–610.

Braisted JE, Tuttle R, O'Leary DD (1999) Thalamocortical axons are influenced by chemorepellent and chemoattractant activities localized to decision points along their path. Dev Biol 208:430–440.

Braisted JE, Catalano SM, Stimac R, Kennedy TE, Tessier-Lavigne M, Shatz CJ, O'Leary DD (2000) Netrin-1 promotes thalamic axon growth and is required for proper development of the thalamocortical projection. J Neurosci 20:5792–5801.

Cases O, Vitalis T, Seif I, De Maeyer E, Sotelo C, Gaspar P (1996) Lack of barrels in the somatosensory cortex of monoamine oxidase A-deficient mice: role of a serotonin excess during the critical period. Neuron 16:297–307.

Chen ZF, Rebelo S, White F, Malmberg AB, Baba H, Lima D, Woolf CJ, Basbaum AI, Anderson DJ (2001) The paired homeodomain protein DRG11 is required for the projection of cutaneous sensory afferent fibers to the dorsal spinal cord. Neuron 31:59–73.

Chiaia NL, Bennett-Clarke CA, Rhoades RW (1991) Effects of cortical and thalamic lesions upon primary afferent terminations, distributions of projection neurons, and the cytochrome oxidase pattern in the trigeminal brainstem complex. J Comp Neurol 303:600–616.

Chiaia NL, Bennett-Clarke CA, Eck M, White FA, Crissman RS, Rhoades RW (1992) Evidence for prenatal competition among the central arbors of trigeminal primary afferent neurons. J Neurosci 12:62–76.

Cohen-Tannoudji M, Babinet C, Wassef M (1994) Early determination of a mouse somatosensory cortex marker. Nature 368:460–463.

Diamond ME, Armstrong-James M, Budway MJ, Ebner FF (1992) Somatic sensory responses in the rostral sector of the posterior group (POm) and in the ventral posterior medial nucleus (VPM) of the rat thalamus: dependence on the barrel field cortex. J Comp Neurol 319:66–84.

Ding YQ, Wang YQ, Qin BZ, Li JS (1993) The major pelvic ganglion is the main source of nitric oxide synthase-containing nerve fibers in penile erectile tissue of the rat. Neurosci Lett 164:187–189.

Dubois L, Vincent A (2001) The COE-Collier/Olf1/EBF-transcription fac-

tors: structural conservation and diversity of developmental functions. Mech Dev 108:3–12.
Erzurumlu RS, Jhaveri S (1992) Trigeminal ganglion cell processes are spatially ordered prior to the differentiation of the vibrissa pad. J Neurosci 12:3946–3955.
Erzurumlu RS, Kind PC (2001) Neural activity: sculptor of 'barrels' in the neocortex. Trends Neurosci 24:589–595.
Gavrieli Y, Sherman Y, Ben-Sasson SA (1992) Identification of programmed cell death in situ via specific labeling of nuclear DNA fragmentation. J Cell Biol 119:493–501.
Hayashi H (1980) Distributions of vibrissae afferent fiber collaterals in the trigeminal nuclei as revealed by intra-axonal injection of horseradish peroxidase. Brain Res 183:442–446.
Henderson TA, Woolsey TA, Jacquin MF (1992) Infraorbital nerve blockade from birth does not disrupt central trigeminal pattern formation in the rat. Brain Res Dev Brain Res 66:146–152.
Henderson TA, Johnson EM, Osborne PA, Jacquin MF (1994) Fetal NGF augmentation preserves excess trigeminal ganglion cells and interrupts whisker-related pattern formation. J Neurosci 14:3389–3403.
Iwasato T, Erzurumlu RS, Huerta PT, Chen DF, Sasaoka T, Ulupinar E, Tonegawa S (1997) NMDA receptor-dependent refinement of somatotopic maps. Neuron 19:1201–1210.
Jacquin MF, Chiaia NL, Haring JH, Rhoades RW (1990) Intersubnuclear connections within the rat trigeminal brainstem complex. Somatosens Mot Res 7:399–420.
Jhaveri S, Erzurumlu RS, Chiaia N, Kumar TR, Matzuk MM (1998) Defective whisker follicles and altered brainstem patterns in activin and follistatin knockout mice. Mol Cell Neurosci 12:206–219.
Killackey HP, Fleming K (1985) The role of the principal sensory nucleus in central trigeminal pattern formation. Brain Res 354:141–145.
Killackey HP, Jacquin MF, Rhoades RW (1990) The somatosensory system. In: Development of sensory systems in mammals (Coleman JR, ed). New York: Wiley.R. W.
Kutsuwada T, Sakimura K, Manabe T, Takayama C, Katakura N, Kushiya E, Natsume R, Watanabe M, Inoue Y, Yagi T, Aizawa S, Arakawa M, Takahashi T, Nakamura Y, Mori H, Mishina M (1996) Impairment of suckling response, trigeminal neuronal pattern formation, and hippocampal LTD in NMDA receptor epsilon 2 subunit mutant mice. Neuron 16:333–344.
Li Y, Erzurumlu RS, Chen C, Jhaveri S, Tonegawa S (1994) Whisker-related neuronal patterns fail to develop in the trigeminal brainstem nuclei of NMDAR1 knockout mice. Cell 76:427–437.
Logan C, Wingate RJ, McKay IJ, Lumsden A (1998) Tlx-1 and Tlx-3 homeobox gene expression in cranial sensory ganglia and hindbrain of the chick embryo: markers of patterned connectivity. J Neurosci 18:5389–5402.
Ma PM (1993) Barrelettes–architectonic vibrissal representations in the brainstem trigeminal complex of the mouse. II. Normal post-natal development. J Comp Neurol 327:376–397.
Mitrovic N, Schachner M (1996) Transient expression of NADPH diaphorase activity in the mouse whisker to barrel field pathway. J Neurocytol 25:429–437.
Molnar Z, Blakemore C (1995) How do thalamic axons find their way to the cortex? Trends Neurosci 18:389–397.
Pereira A, Freire MAM, Bahia CP, Franca JG, Picanco-Diniz CW (2000) The barrel field of the adult mouse SmI cortex as revealed by NADPH-diaphorase histochemistry. Neuroreport 11:1889–1892.
Qian Y, Shirasawa S, Chen CL, Cheng L, Ma Q (2002) Proper development of relay somatic sensory neurons and D2/D4 interneurons requires homeobox genes Rnx/Tlx-3 and Tlx-1. Genes Dev 16:1220–1233.
Rebsam A, Seif I, Gaspar P (2002) Refinement of thalamocortical arbors and emergence of barrel domains in the primary somatosensory cortex: a study of normal and monoamine oxidase a knock-out mice. J Neurosci 22:8541–8552.
Saito T, Greenwood A, Sun Q, Anderson DJ (1995) Identification by differential RT-PCR of a novel paired homeodomain protein specifically expressed in sensory neurons and a subset of their CNS targets. Mol Cell Neurosci 6:280–292.
Senft SL, Woolsey TA (1991) Growth of thalamic afferents into mouse barrel cortex. Cereb Cortex 1:308–335.
Shortland PJ, Demaro JA, Shang F, Waite PM, Jacquin MF (1996) Peripheral and central predictors of whisker afferent morphology in the rat brainstem. J Comp Neurol 375:481–501.
Tracey DJ, Waite PME (1995) Somatosensory system. In: The rat nervous system (Paxinos G, ed). San Diego: Academic.
Wang MM, Reed RR (1993) Molecular cloning of the olfactory neuronal transcription factor Olf-1 by genetic selection in yeast. Nature 364:121–126.
Wang SS, Tsai RYL, Reed RR (1997) The characterization of the Olf-1/EBF-like HLH transcription factor family: implications in olfactory gene regulation and neuronal development. J Neurosci 17:4149–4158.
Williams MN, Zahm DS, Jacquin MF (1994) Differential foci and synaptic organization of the principal and spinal trigeminal projections to the thalamus in the rat. Eur J Neurosci 6:429–453.
Willis WD, Coggeshall RE (1991) Sensory mechanisms of the spinal cord. London: Plenum.
Wong-Riley MT, Welt C (1980) Histochemical changes in cytochrome oxidase of cortical barrels after vibrissal removal in neonatal and adult mice. Proc Natl Acad Sci USA 77:2333–2337.
Woolsey TA (1990) Peripheral alteration and somatosensory development. In: Development of sensory systems in mammals (Coleman JR, ed), pp 461–516. New York: Wiley.
Woolsey TA, Van der Loos H (1970) The structural organization of layer IV in the somatosensory region (SI) of mouse cerebral cortex. The description of a cortical field composed of discrete cytoarchitectonic units. Brain Res 17:205–242.